

# polymer papers

## Mechanical properties of thermotropic liquid crystalline polyesters and polyamides

H. Zhang, G. R. Davies and I. M. Ward\*

IRC in Polymer Science and Technology, University of Leeds, Leeds, LS2 9JT, UK  
(Received 25 June 1991; accepted 1 October 1991)

The dynamic mechanical behaviour of highly oriented tapes and monofilaments of thermotropic liquid crystalline polymers based on hydroxynaphthoic acid, terephthalic acid and either aminophenol (designated HNATA) or hydroquinone (designated HNATH) have been studied in tension and torsion. It was found that the mechanical properties of these two polymers were very similar. In the case of HNATA both the tensile modulus and the chain modulus determined from X-ray diffraction measurements were studied as a function of applied stress. The aggregate model, when extended to include non-linearity, modelled the macroscopic tensile and shear behaviour with some success. The X-ray measurements could not be reconciled with the macroscopic measurements, which is tentatively attributed to the fact that these materials possess a complex hierarchical morphology.

(Keywords: thermotropic liquid crystalline polymers; mechanical behaviour)

### INTRODUCTION

This work is part of an ongoing study of thermotropic liquid crystal polymers in which we aim to achieve an understanding of the mechanical properties of the materials in terms of their structure. We have previously studied random copolyesters of hydroxybenzoic acid and hydroxynaphthoic acid<sup>1</sup> or similar materials<sup>2</sup> including biphenyl, terephthalic acid or dihydroxynaphthalene. Though sounding chemically very different, all compositions form polymers which are basically benzene or naphthalene rings linked by ester linkages. These flexible ester linkages allow processing in conventional melt extrusion machinery but decrease the maximum working temperature which can be achieved in similar amide-linked materials (cf. Kevlar). Our present aim is to study a material with mixed ester and amide linkages produced by incorporation of aminophenol to determine whether an enhancement in properties could be obtained whilst retaining melt processibility. In particular, it was thought that hydrogen bonding might substantially improve the shear modulus<sup>3</sup> and hence the tensile modulus through its dependence on the shear modulus<sup>1</sup>.

The partially amide-linked material which we have studied is referred to as HNATA. For comparison, we have also studied a similar polymer with all ester linkages which we refer to as HNATH. The compositions of these materials are summarized in *Table 1*. The amide content of HNATA, which corresponds to one-fifth of the linkages, is close to the maximum content tolerable from a melt processibility standpoint and 60% HNA gives the lowest melting point<sup>3</sup> of about 280°C.

### EXPERIMENTAL

#### Sample preparation

The copolyester/amide and copolyester investigated in

this work, HNATA and HNATH, were supplied by the Hoechst-Celanese Research Company. Two types of specimen were provided: highly oriented monofilaments of about 1 mm diameter and thin tapes about 20  $\mu\text{m}$  (HNATA) or 10  $\mu\text{m}$  (HNATH) thick and 5 mm wide. Both sets of samples were freely annealed in nitrogen. Details of the chemical composition and annealing treatment are given in *Table 1*. The samples were produced by spinning from the melt with an extensional flow field sufficient to induce high orientation, which was confirmed by wide angle X-ray scattering (WAXS) photography. The thin tapes were designed to give a stiffness appropriate for isochronal creep, dynamic tensile and X-ray modulus measurements. The monofilaments gave a torsional rigidity adequate for shear measurements in a torsion pendulum apparatus.

#### Creep measurements

Measurements were made using the dead-loading extensional creep apparatus similar to that described by Gupta and Ward<sup>4</sup>. Samples about 60 mm long and 1 mm wide were cut from the thin oriented tapes. They were conditioned by repeatedly applying the maximum load at 150°C (the highest temperature studied) with an appropriate recovery time prior to taking any measure-

Table 1 Composition of the liquid crystal copolyesters

	Composition (mol%) <sup>a</sup>				Heat treatment	
	HNA	TA	AM	HQ	Time (h)	Temp. (°C)
HNATA	60	20	20		4 15	250 270
HNATH	60	20		20	4 15	250 270

<sup>a</sup>HNA = hydroxynaphthoic acid; TA = terephthalic acid; AM = amino-phenol; HQ = hydroquinone

\*To whom correspondence should be addressed

ments. The maximum stress applied to HNATA samples at high temperatures was 0.4 GPa and samples recovered well allowing extensive study of their non-linear stress-strain response. The HNATH samples were much weaker, however, and the maximum stress which could safely be applied to them was 50 MPa. This did not produce measurable non-linearity.

#### Dynamic shear measurements

These were performed on the oriented rods in a home-made inverted torsion pendulum apparatus<sup>5,6</sup>. In view of the small diameter of the samples (~1 mm) and low shear modulus at high temperatures, a very light torsion arm was used but periods of several seconds still resulted.

#### Dynamic tensile measurements

Dynamic measurements were made on a direct dynamic tension apparatus similar to that described previously<sup>2</sup> using samples which were similar to those used for creep measurements. In addition to varying temperature and frequency, dynamic data were also obtained at different levels of static stress. Samples were again conditioned at 150°C under the highest static stress for about 30 min before taking any readings.

#### X-ray compliance measurements

The X-ray compliance is normally obtained for crystalline polymers by deducing the lattice strain from the shift in diffraction angle when a stress is applied. In this case, however, we are dealing with a random copolymer with little conventional crystallinity. Nevertheless, the meridional diffraction pattern has strong aperiodic peaks which are well understood<sup>7</sup> and the shift in these peaks can be used as a measure of strain in the chain direction to generate an X-ray compliance. Note, however, that all chains can contribute to this measurement, not just those in crystalline regions, and the width of the meridional peaks implies that the X-rays are 'seeing' sections of chain of the order of 10 monomers long.

Film samples 10–20 μm thick, 5 mm wide and 60 mm long were used in the X-ray measurements. They were mounted in an environmental chamber which could vary the sample temperature from –80°C to 160°C in an atmosphere of dry nitrogen. A lever arrangement allowed loads of several kilograms to be applied to the samples. Conditioning procedures were used, as described for the creep measurements.

The diffracted X-rays were detected by a linear position-sensitive detector<sup>8</sup> which allowed the collection of data over the whole peak profile simultaneously. Typical collection times were about 40 s followed by 3–5 min with the sample unloaded to allow it to recover to its original state. The meridional peak used for analysis was that at  $d = 2.1 \text{ \AA}$  ( $2\theta = 43^\circ$  with Cu K $\alpha$  radiation). A detailed description of the apparatus and the method are given in a previous paper<sup>9</sup>.

#### Thermal expansion measurements

The apparatus for the axial thermal expansion measurements was described previously<sup>10</sup>. Tape samples about 50 mm in length were suspended in a fused silica tube through which flowed a stream of temperature-controlled nitrogen gas. A light rod carrying the slug of

a linear variable differential transformer was attached to a clamp at the lower end of the sample. The change in temperature and the accompanying change in sample length were recorded on an X-Y recorder. The sample was conditioned for 1 h at 160°C under a light tensile stress of about 2 MPa to keep it straight. The temperature was then cycled by  $\pm 5^\circ\text{C}$  at mean temperatures varying from –80°C to 160°C.

At high temperatures, a small correction was made to account for the change in modulus with temperature which produced a change in strain due to the 2 MPa dead load.

## RESULTS

#### Creep measurements

Typical stress-strain curves for HNATA at different temperatures are shown in *Figure 1*. These data clearly show increasing non-linearity at higher temperatures. As can be seen by the solid lines in *Figure 1*, the data can be well represented by the expression:

$$\varepsilon = J_\infty \sigma + k[1 - \exp(-B\sigma)] \quad (1)$$

where  $\sigma$  is the stress,  $\varepsilon$  the strain and  $J_\infty$ ,  $k$  and  $B$  are fitting parameters. This implies that as  $\sigma$  tends to infinity a constant value of  $\partial\varepsilon/\partial\sigma$  ( $= J_\infty$ ) results, i.e. the incremental compliance asymptotically approaches a high stress limit.

#### Dynamic shear measurements

The dynamic shear results are shown in *Figures 2* and *3* for HNATA and HNATH, respectively. It can be seen that the positions of the relaxations are similar in both materials but that HNATA (with amide linkages) has a slightly increased shear modulus at low temperatures. The effect is small, however, and may well be due to differences in chain orientation and not directly due to the possible hydrogen bonding in HNATA.

It was thought possible that water absorption might affect the hydrogen bonding, as with nylon 66<sup>11</sup>. The comparison was therefore made between a wet sample of HNATA (soaked in water at room temperature for 72 h) and a dry sample (dried in an air oven at 110°C for 72 h). No difference was observed between the shear properties of the two samples.

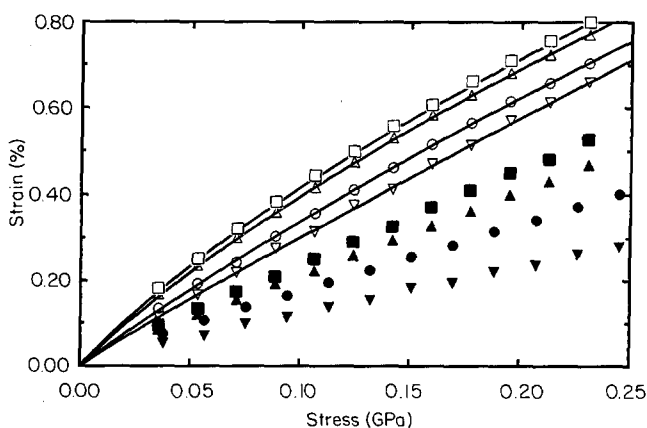


**Figure 1** Creep data for HNATA at different temperatures:  $\nabla$ , –40°C;  $\bullet$ , 20°C;  $\blacktriangle$ , 60°C;  $\blacksquare$ , 80°C;  $\nabla$ , 120°C;  $\circ$ , 130°C;  $\triangle$ , 140°C;  $\square$ , 150°C

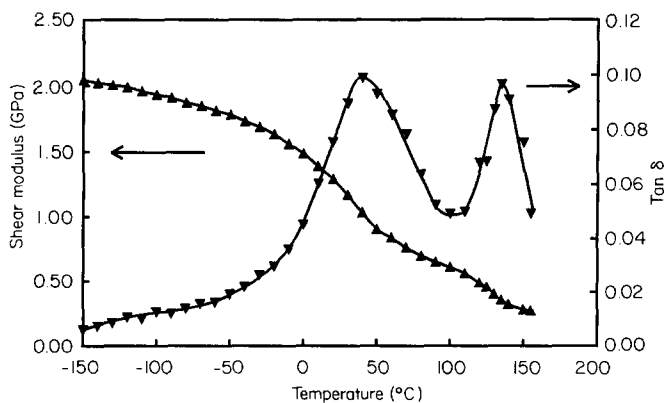


Figure 2 Dynamic shear modulus and  $\tan \delta$  of HNATA at 0.2–0.5 Hz

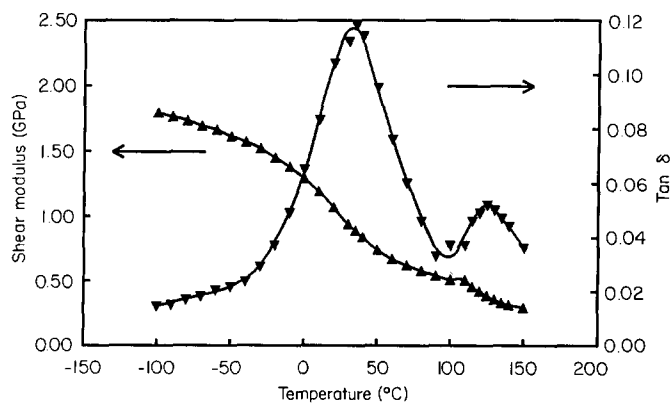


Figure 3 Dynamic shear modulus and  $\tan \delta$  of HNATH at 0.2–0.5 Hz

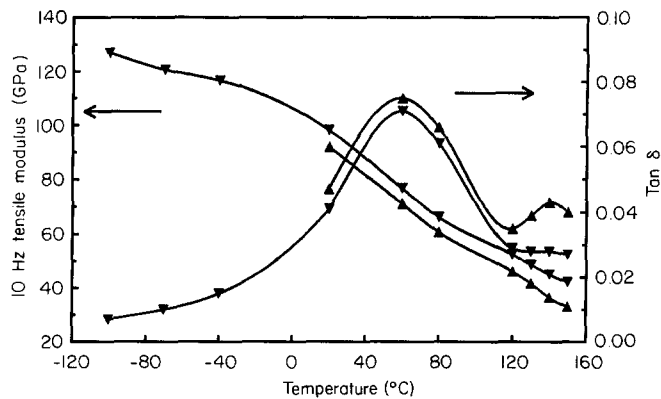


Figure 4 Dynamic tensile modulus at 10 Hz and  $\tan \delta$  of HNATA as a function of temperature at different static stresses:  $\blacktriangle$ , 65 MPa;  $\blacktriangledown$ , 165 MPa

Dynamic tensile measurements

Figure 4 shows dynamic tensile data for HNATA at 10 Hz as a function of temperature at two different static stresses. Figure 5 shows similar data for HNATH at a single static stress of 36 MPa. Clearly, the HNATH sample has a lower tensile modulus than the HNATA sample but this difference is slight and could be due to a difference in orientation rather than any intrinsic molecular stiffness.

It can be seen that the HNATA data are stress dependent and that the high temperature  $\alpha$  relaxation is suppressed by the static stress. An alternative view of the non-linearity is shown in Figure 6 where the 10 Hz dynamic compliance of HNATA is plotted as a function

of static stress at different temperatures. It is readily seen that the material becomes increasingly non-linear at temperatures around the  $\alpha$  ( $T_g$ ) relaxation. These data are fitted with a modification of equation (1) obtained by differentiation:

$$J = \partial \epsilon / \partial \sigma = J_\infty + A \exp(-B\sigma) \quad (2)$$

Alternatively, we can introduce the parameter  $J_0$ , the extrapolated compliance at zero static stress ( $J_0 = J_\infty + A$ ) to represent the dynamic compliance of the unstressed sample:

$$J = J_\infty + (J_0 - J_\infty) \exp(-B\sigma) \quad (3)$$

The solid lines in Figure 6 are obtained by fitting equations (2) and (3) to the data at different temperatures. The fitting parameters are summarized in Table 2. These data, by extrapolating to zero and infinite static stress, emphasize the large difference between the low and high stress compliance at high temperatures.

The dynamic tensile data proved difficult to obtain with any precision around room temperature due to the large  $\beta$  relaxation which resulted in non-negligible creep during the loading cycle. Also, at low temperatures, the data were obtained at stresses where  $B\sigma < 1$  giving relatively little curvature and hence, although  $J_0$  is reasonably accurate, the other parameters were difficult to determine with any accuracy.

X-ray compliance measurements

Typical X-ray ‘stress–strain’ curves for HNATA are shown in Figure 7 and the temperature dependence of

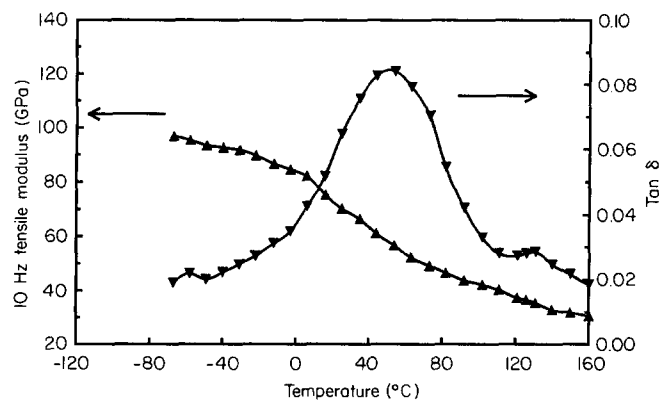


Figure 5 Dynamic tensile modulus at 10 Hz and  $\tan \delta$  of HNATH as a function of temperature at 36 MPa static stress

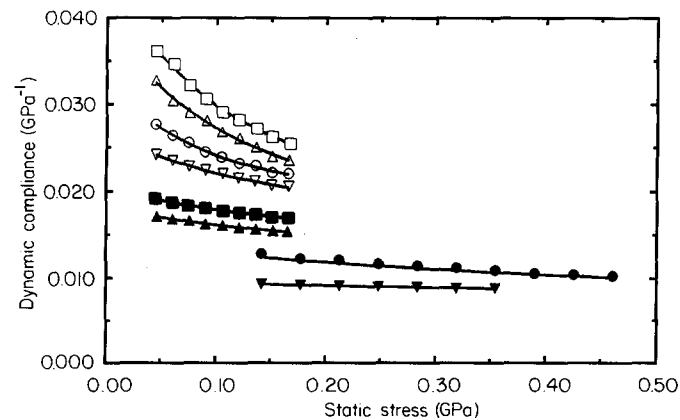
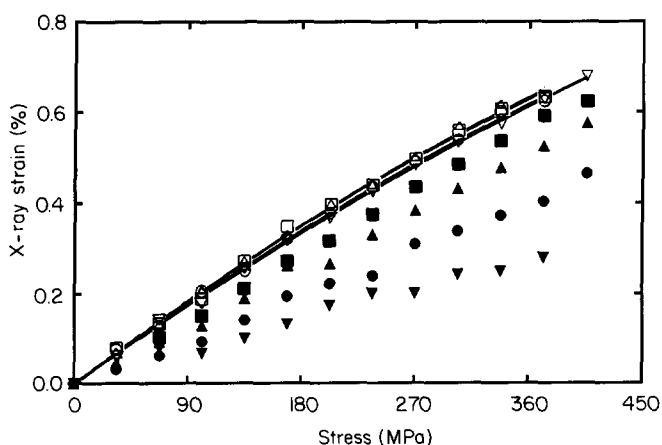


Figure 6 The dynamic compliance of HNATA as a function of static stress at different temperatures: key as for Figure 1

**Table 2** Fitted parameters for HNATA. The 'Low  $f$ ' data were obtained at frequencies 0.2–0.5 Hz to match the shear data. ( $1 \text{ TPa}^{-1} = 10^{-12} \text{ m}^2 \text{ N}^{-1}$ )

Temp. (°C)	$J_{\infty}$ (TPa <sup>-1</sup> )		$A$ (TPa <sup>-1</sup> )		$J_0$ (TPa <sup>-1</sup> )		$B$ (GPa <sup>-1</sup> )	
	Low $f$	10 Hz	Low $f$	10 Hz	Low $f$	10 Hz	Low $f$	10 Hz
150	21	20	24.4	20	45.4	40	11	10
140	19	18	20.2	16	39.2	34	9	8
130	20.1	17	12.7	11	32.8	28	12	8
120	17.9	17	8.7	8.3	26.6	25.3	7	8
80	15.3	15	5.3	3.7	20.3	18.7	7	10
60	14.0	13	4.3	3.4	18.3	16.4	7	9
20	8	7.4	6.6	5.4	14.6	12.8	3	2
-40	8.2	8.4	1.8	2.1	10.0	10.5	2	15
-60	8.4	8.4	1.6	1.9	10.0	10.3	7	7
-100	8.3	7.4	1.4	1.1	9.7	8.5	19	6



**Figure 7** X-ray stress–strain data for HNATA at different temperatures: key as for Figure 1

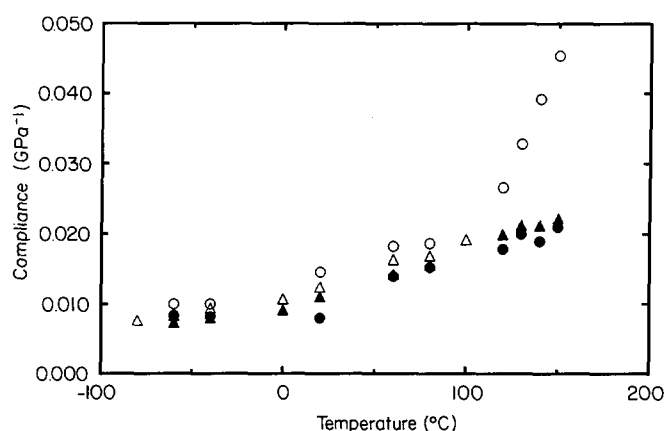


**Figure 8** Temperature dependence of X-ray compliance of HNATA (▲) and HNATH (△) compared with the dynamic  $J_0$  (○) and  $J_{\infty}$  (●) of HNATA

the X-ray compliance derived from the initial slope is shown in Figure 8 for both HNATA and HNATH (where data were obtained at low stresses only). It can be seen that, yet again, there is very little difference between the properties of the two polymers.

Also shown in Figure 8 are the extrapolated macroscopic compliances  $J_0$  and  $J_{\infty}$  listed in Table 2. The similarity between  $J_{\infty}$  and the X-ray compliance is most surprising since the X-ray data are derived from the initial slope of the stress–strain curve and might be expected to correlate with  $J_0$  rather than  $J_{\infty}$ .

Returning to the X-ray compliance data of Figure 7, non-linearity is obvious at high temperatures but we were unable to fit the curves with an equation of the form of equation (1). Simple parabolic fits are mathematically adequate but clearly cannot sensibly be extrapolated to infinite stress. This implies that the X-ray non-linearity is not of the same origin as the macroscopic non-linearity. It is also significant that these data are relatively constant in the region 120–150°C but that the equivalent macroscopic creep data (Figure 1) vary a great deal in this region, again emphasizing the difference between the X-ray and macroscopic data.

*Thermal expansion measurements*

The axial thermal expansion coefficients for HNATA and HNATH are plotted as a function of temperature in

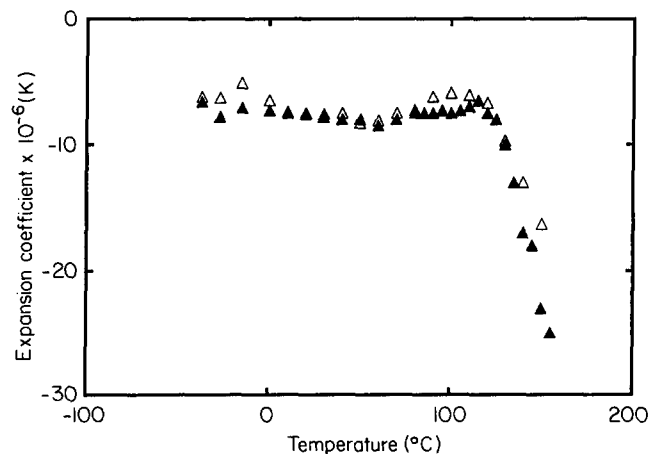


**Figure 9** Axial thermal expansion coefficient of HNATA (▲) and HNATH (△) as functions of temperature

Figure 9. Again, little difference can be seen between the two polymers. Similar results were reported for several related copolyesters by Green *et al.*<sup>12</sup>. The negative value of the axial thermal expansion coefficient at low temperatures is typical of highly oriented linear polymers and is due to thermal libration and bending modes which shorten the chain as the temperature is increased. The

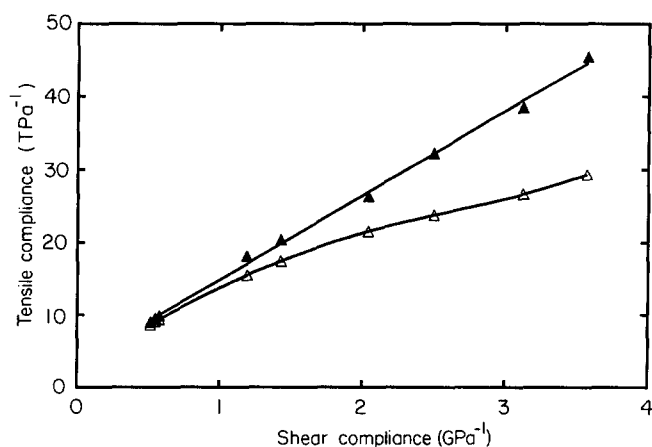


**Figure 10** Dynamic compliance at 10 Hz of HNATA plotted versus  $1/G$  as suggested by the simple aggregate model: ▲,  $J$  extrapolated to zero stress; △, raw data obtained at a static stress of 100 MPa

increasingly negative values above  $T_g$  presumably arise from changes in chain conformation which are frozen out below  $T_g$ . These changes in conformation produce changes in orientation of sections of the chain which in turn affects the mechanical properties, as explained below.

## THEORY

### The aggregate model (linear)

The aggregate model of Ward<sup>13</sup> can be simplified for the special case of highly anisotropic uniaxially aligned polymers<sup>1</sup> to give the simple relationship:

$$J = J_u + \frac{\langle \sin^2(\theta) \rangle}{G} \quad (4)$$

In this representation,  $J_u$  is the tensile compliance of a unit of structure along its axis of cylindrical symmetry,  $G$  is the macroscopic shear modulus of the sample (obtained by torsion about its symmetry axis),  $\theta$  is the angle between the symmetry direction of the unit and the sample, and the angular brackets imply averaging over all units.

We have previously used this relationship to relate tensile and shear data for the copolyesters with some success<sup>2,14</sup>. Figure 10 shows that a linear plot is again produced for HNATA if we plot  $J_0$  against  $1/G$ , where  $J_0$  is the extrapolated dynamic compliance at zero stress and  $G$  is the shear modulus at the same frequency. The slope of this plot yields a  $\langle \sin^2(\theta) \rangle$  value of 0.0116. This corresponds to a  $\theta$  value of only  $6^\circ$  and similar values are obtained for HNATH. Clearly our 'units of structure', whatever their physical origin, are highly aligned. The intercept at  $1/G = 0$  yields a tensile modulus for the units of 295 GPa which is much greater than the measured X-ray modulus at any temperature but comparable with the theoretical modulus of similar monomers<sup>9</sup>.

The significance of this type of data, obtained on many different copolyesters, is further discussed in a previous paper<sup>2</sup>. In this paper we concentrate upon the non-linearity of the response.

### Extension of the model to include non-linearity

The inadequacy of the modelling is seen in Figure 10 where the raw data obtained under a constant 100 MPa

static stress deviate markedly from the extrapolated zero stress data. The change in slope of the raw data implies that  $\langle \sin^2(\theta) \rangle$  reduces as the compliances increase, i.e. the static stress is producing a higher alignment of the units at higher temperatures. We might therefore expect that at constant temperature an increase in static stress produces an alignment of the units expressed by a relationship such as:

$$\langle \sin^2(\theta) \rangle = \langle \sin^2(\theta) \rangle_0 \exp(-B\sigma) \quad (5)$$

where  $\langle \sin^2(\theta) \rangle_0$  is the orientation in the absence of an applied stress, since we expect that  $\langle \sin^2(\theta) \rangle$  must change asymptotically to zero as the tensile stress is increased.

Two studies have treated this problem. Allen and Roche<sup>15</sup> derive:

$$\langle \tan^2(\theta) \rangle = \langle \tan^2(\theta) \rangle_0 \exp(-2\sigma/G_s) \quad (6)$$

where  $G_s$  is the static shear modulus. Northolt and van der Hout<sup>16</sup>, however, derive:

$$\langle \tan^2(\theta) \rangle = \langle \tan^2(\theta) \rangle_0 \exp(-\sigma/G_s) \quad (7)$$

At the high orientations at which we are working we can neglect the difference between  $\langle \sin^2(\theta) \rangle$  and  $\langle \tan^2(\theta) \rangle$  and write a general modified form of equation (4):

$$J = J_\infty + \frac{\langle \sin^2(\theta) \rangle_0}{G} \exp(-B\sigma) \quad (8)$$

where  $B$  is  $1/G_s$  or  $2/G_s$  and our fitting parameters from equations (2) and (3) are given by:

$$A = J_0 - J_\infty = \langle \sin^2(\theta) \rangle_0 / G \quad (9)$$

### Estimation of $\langle \sin^2(\theta) \rangle_0$ changes from thermal expansion

Few authors have correlated the negative thermal expansion coefficient of liquid crystal polymers with their molecular orientation<sup>17,18</sup>. A simple relationship between thermal expansion coefficient and the orientation parameter can, however, be obtained by assuming that highly aligned units are joined end to end, i.e. the sample length is given by the summation of the length of  $N$  misaligned units projected along the sample symmetry axis. Hence:

$$l = \sum L \cos(\theta_i) = NL \langle \cos(\theta) \rangle_0 \quad (10)$$

where  $l$  is the sample length,  $L$  is the unit length and  $\theta_i$  is the orientation angle of the  $i$ th unit.

The thermal expansion coefficient is then given by:

$$\begin{aligned} \alpha_T &= \frac{1}{l} \left( \frac{\partial l}{\partial T} \right)_\sigma \\ &= \frac{1}{L} \left( \frac{\partial L}{\partial T} \right)_\sigma + \frac{1}{\langle \cos(\theta) \rangle_0} \left( \frac{\partial \langle \cos(\theta) \rangle_0}{\partial T} \right)_\sigma \end{aligned} \quad (11)$$

If every  $\theta_i$  is small then  $\cos(\theta_i) \approx 1 - [\sin^2(\theta_i)]/2$  and  $\langle \cos(\theta) \rangle_0 \approx 1$ . Hence:

$$\alpha_T = \alpha_0 - \frac{1}{2} \frac{\partial \langle \sin^2(\theta) \rangle_0}{\partial T} \quad (12)$$

where  $\alpha_0$  is the contribution from the change in length of the units. We may therefore estimate changes in  $\langle \sin^2(\theta) \rangle_0$  from:

$$\langle \sin^2(\theta) \rangle_0 = S_0 + 2 \int^\tau (\alpha_0 - \alpha_T) dT \quad (13)$$

**Table 3** A comparison of  $2/B$  (Allen model) and  $1/B$  (Northolt model) with the measured shear modulus reduced to low frequencies ( $G_s$ )

Temperature (°C)	$2/B$ (GPa)	$G_s$ (GPa)	$1/B$ (GPa)
150	0.21 (3)	0.22	0.11 (1)
140	0.22 (4)	0.24	0.11 (2)
130	0.17 (2)	0.30	0.09 (1)
120	0.27 (8)	0.40	0.14 (4)
80	0.28 (4)	0.56	0.14 (2)
60	0.29 (7)	0.6	0.15 (3)
20	0.8 (2)	0.9	0.4 (1)
-40	0.8 (2)	1.6	0.4 (1)
-60	0.29 (7)	1.7	0.15 (4)

The value in parentheses is the error in the last figure

where  $S_0$  is an arbitrary constant. We identify  $\alpha_0$  with the essentially constant coefficient seen below  $T_g$  and can choose  $S_0$  to set a given value of  $\langle \sin^2(\theta) \rangle_0$  at a particular temperature.

**DISCUSSION**

In the non-linear aggregate model described above, the non-linearity arises from the rotation of the units as the tensile stress is increased. The Allen and Northolt models for this rotation differ in their predictions for the value of the coefficient  $B$  in equation (8). Allen predicts that  $B = 2/G_s$  whereas Northolt predicts  $B = 1/G_s$ . Unfortunately, we do not have the 'static' or very low frequency measurements of the shear modulus required to check these predictions. We have, however, used the Alfrey approximation<sup>19</sup>:

$$\frac{\Delta G(\omega)}{\Delta \ln(\omega)} = \frac{2}{\pi} G''(\omega)$$

to estimate the shear modulus at a creep time of 500 s from our dynamic data taken at 0.2–0.5 Hz. This time was chosen to represent a typical loading time prior to taking dynamic measurements.

When the extrapolated  $G_s$  is compared with  $1/B$  (Northolt) and  $2/B$  (Allen) in Table 3 we see that the Northolt model does not fit at any temperature but that, though failing to fit at low temperatures, the Allen model fits well in the region of  $T_g$  where the shear modulus has fallen to levels comparable with the maximum stress which can be applied.

A simple model, based on the nematic texture and the extreme anisotropy of the mechanical properties of the material in this temperature range, can readily illustrate the rotation of the units to yield the Allen result. We imagine the sample to consist of sinuous chains or fibrils which attempt to pack in 'parallel curves' as illustrated in Figure 11. A tensile stress causes a straightening of the chains which requires the inclined portions to simultaneously rotate and shear. This is more clearly seen if we consider the zig-zag model also shown in the figure.

If, for simplicity, we assume that the chains are inextensible and remain a constant distance apart then the shear strain  $\gamma$  is given by:

$$\gamma = \frac{BC}{OC} = \frac{AC - AB}{OC} \tag{14}$$

hence:

$$\gamma = -[\tan(\theta) - \tan(\theta_0)] \tag{15}$$

or, in differential form:

$$\delta\gamma = -\delta[\tan(\theta)] = -\sec^2(\theta) \delta\theta \approx -\delta\theta \tag{16}$$

For small  $\theta$  we see therefore that  $\delta\gamma = -\delta\theta$ . That is, the shear strain and rotation of the unit are equal in magnitude but opposite in direction.

If this deformation is caused by a tensile stress  $\delta\sigma$  applied along the axis of the zig-zag then the appropriately resolved shear stress is  $\delta\sigma \sin(\theta) \cos(\theta)$  and, writing  $G$  for the shear modulus, we have:

$$\delta\gamma = \delta\sigma \frac{\sin(\theta) \cos(\theta)}{G} = -\delta\theta \tag{17}$$

Hence:

$$\int \frac{d\sigma}{G} = - \int \frac{d\theta}{\sin(\theta) \cos(\theta)} \tag{18}$$

With the boundary condition that  $\theta = \theta_0$  at  $\sigma = 0$  this integrates to give:

$$\tan(\theta) = \tan(\theta_0) e^{-\sigma/G} \tag{19}$$

which is the result derived by Allen<sup>15</sup> and quoted in squared form as equation (6).

If the length of the unit is  $L$  then  $l$ , the projected length along the axis of the zig-zag, is  $L \cos(\theta)$ . The tensile strain  $\delta\epsilon$  is therefore given by:

$$\delta\epsilon = \frac{\delta l}{l} = -\tan(\theta) \delta\theta \tag{20}$$

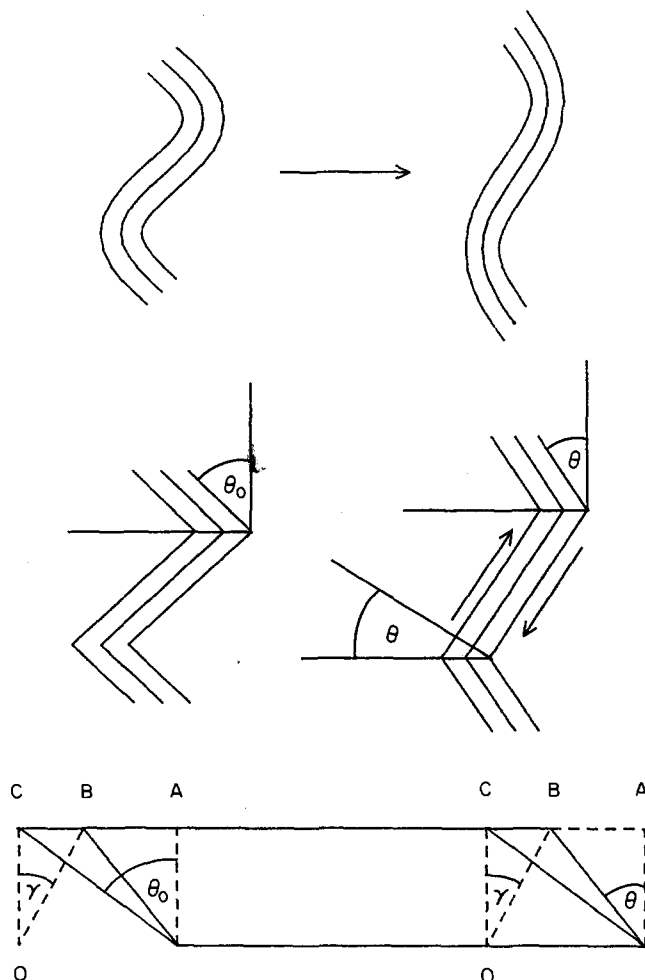


**Figure 11** Simple structural model

Using equation (17) to relate  $\delta\theta$  to  $\delta\sigma$  we therefore see that the incremental tensile compliance  $J$  is given by:

$$J = \frac{\delta\varepsilon}{\delta\sigma} = \frac{\sin^2(\theta)}{G} = \frac{\sin^2(\theta)_0}{G} \exp(-2\sigma/G) \quad (21)$$

in agreement with the aggregate model since we have neglected the tensile deformation of the units which is the origin of  $J_\infty$  in equation (8).

Unfortunately, this simple model fails to explain the X-ray observations that the low stress X-ray compliance is similar to the extrapolated high stress macroscopic compliance and that the X-ray non-linearity is of a smaller magnitude and different character to the macroscopic non-linearity. Since the X-ray strain measurements essentially measure the change in the average projected length of the chains and the macroscopic measurements are related simply to the sum of the projected lengths, there can be no difference between the X-ray strain and the macroscopic strain if it is assumed that the X-ray measurements relate to the whole sample.

It was thought possible that the X-ray measurements were biased towards those chains which are aligned in the draw direction ( $\theta = 0^\circ$ ) since measurements are taken along the meridian and not over the whole diffraction 'streak'. They would then tend to reflect the 'fully aligned' situation which the macroscopic measurements tend to at high stress and not contain the non-linear contribution from the change in average alignment with stress. Additional experiments performed  $5^\circ$  off the meridian gave similar results, however, and this hypothesis was therefore rejected.

We must therefore conclude that either the X-ray technique is not measuring the change in the average projected length of the chains or the simple model described above is incapable of predicting a difference between the X-ray and macroscopic non-linearities and a more complicated model is required. A suitable modification to a single phase model is not readily apparent. If the relation between shear angle  $\gamma$  and rotation angle  $\theta$  (equation (16)) is modified then the exact correspondence between macroscopic and X-ray strains would be relaxed but the coefficient  $B$  would no longer be  $1/2G$  as predicted in the Allen model and found by experiment to be applicable above  $T_g$ .

Irrespective of the detailed modelling, it is clear that the initial orientation of the units as expressed by  $\langle \sin^2(\theta) \rangle_0$  controls the mechanical properties of the sample. It is not obvious, however, whether  $\langle \sin^2(\theta) \rangle_0$  varies with temperature. We have several ways of attempting to determine this.

- Using equation (9) we can calculate  $\langle \sin^2(\theta) \rangle_0$  from the data in Table 2 and the measured dynamic shear modulus.
- We can identify  $J_\infty$  with the tensile compliance of the units determined by X-ray measurements ( $J_x$ ) and calculate  $\langle \sin^2(\theta) \rangle_0$  from:

$$\langle \sin^2(\theta) \rangle_0 = ({}^iJ_0 - J_x) * G$$

where  ${}^iJ_0$  is the measured creep ( ${}^cJ_0$ ) or dynamic ( ${}^dJ_0$ ) compliance, extrapolated to  $\sigma = 0$ . (For the dynamic data,  $J$  and  $G$  were obtained at the same frequency. For the creep data, however,  $G$  must be corrected to the equivalent frequency of the creep measurement using the Alfrey approximation.)

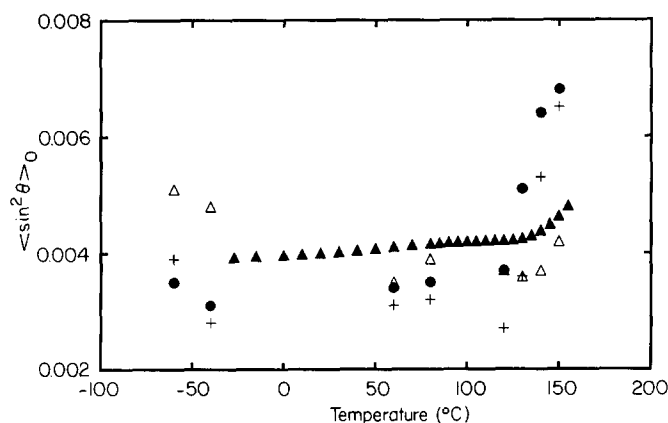


Figure 12 Alternative measures of  $\langle \sin^2(\theta) \rangle_0$  as a function of temperature: ●, from GA; +, from  $G({}^dJ_0 - J_x)$ ; Δ, from  $G({}^cJ_0 - J_x)$ ; ▲, from thermal expansion

- We can estimate the temperature dependence of  $\langle \sin^2(\theta) \rangle_0$  from the measured  $\alpha_T$  using equation (13).

It can be seen from Figure 12 that these calculations yield similar values of  $\langle \sin^2(\theta) \rangle_0$  which, though scattered, appear to vary with temperature in the region of the glass transition. This is at odds with our previous simple analyses which have assumed a constant  $\langle \sin^2(\theta) \rangle_0$  but the change may only be significant above the glass transition. We are currently investigating methods of measurement of  $\langle \sin^2(\theta) \rangle_0$  by X-ray or i.r. techniques to independently verify these observations.

These values of  $\langle \sin^2(\theta) \rangle_0$  are significantly less than the value of 0.0116 deduced from the simple plot of  $J$  versus  $1/G$  (Figure 10). As discussed elsewhere<sup>2</sup>, we believe that the simple plot which assumes temperature-independent unit parameters essentially relates to an average monomer. The values of  $\langle \sin^2(\theta) \rangle_0$  plotted in Figure 12 must relate to larger units which contain many monomers since larger units<sup>2</sup> necessarily have a smaller value of  $\langle \sin^2(\theta) \rangle_0$ .

We see, therefore, that the parameters resulting from fitting the non-linear aggregate model in this way are probably not applicable at the molecular level and that the units which are aligned by the applied stress contain many monomers. In view of the fibrillar texture displayed by such materials<sup>20,21</sup>, it is highly probable that the stress tends to align fibrils rather than individual chains. It must be remembered, however, that the non-linear mechanical behaviour is not reflected by the X-ray measurements under stress. We therefore conclude that there is a contribution to the macroscopic compliance which we have not been able to relate directly to the deformation (i.e. extension, shear and rotation) of structural units (at any level) during a homogeneous deformation. This could arise from the complex hierarchical morphology of these materials (which are akin to fibrils within an overall twisted structure like cords within a rope) so that, in addition to the deformation of the units registered by X-ray measurements, such units are sliding over themselves.

## CONCLUSIONS

We see that partial substitution of amide linkages for ester linkages on the scale studied here produces little

difference in the mechanical properties of the highly oriented material. If higher working temperatures are required then melt processibility must be sacrificed.

The aggregate model, when extended to include non-linearity, can model the macroscopic behaviour and Allen's model<sup>15</sup> gives the best correlation between the shear modulus deduced from the non-linear stress/strain data and that measured experimentally in the region of the glass transition. Both Allen's and Northolt's<sup>16</sup> models fail to fit the data obtained below the glass transition.

X-ray measurements yield results which are different in character from the macroscopic measurements. This may be due to the experimental X-ray technique or it may point to a fundamental inadequacy of the modelling.

A number of indirect measurements suggest that the orientation of the units in the unstressed state changes with temperature, particularly above the glass transition.

## REFERENCES

- 1 Davies, G. R. and Ward, I. M. in 'High Modulus Polymers' (Eds A. E. Zachariades and R. S. Porter), Marcel Dekker, New York, 1988
- 2 Green, D. I., Unwin, A. P., Davies, G. R. and Ward, I. M. *Polymer* 1990, **31**, 579
- 3 Calundann, G. W. and Jaffe, M. 'Proceedings of the Robert A. Welch Foundation Conference on Chemical Research, XXVI. Synthetic Polymers', Houston, Texas, 1982
- 4 Gupta, V. B. and Ward, I. M. *J. Macromol. Sci. (Phys.)* 1967, **B1**(2), 373
- 5 Heijboer, J., Deking, P. and Staverman, A. J. Proc. 2nd Int. Cong. Rheology, Butterworth, London, 1954, pp. 123-133
- 6 Green, D. I. *PhD Thesis*, University of Leeds, 1989
- 7 Blackwell, J., Gutierrez, G. A. and Chivers, R. A. *Macromolecules* 1984, **17**, 1219
- 8 Thistlethwaite, T., Jakeways, R. and Ward, I. M. *Polymer* 1988, **29**, 61
- 9 Troughton, M. J., Unwin, A. P., Davies, G. R. and Ward, I. M. *Polymer* 1988, **29**, 1389
- 10 Orchard, G. A. J., Davies, G. R. and Ward, I. M. *Polymer* 1984, **25**, 1203
- 11 Abdul-Jawad, S. *PhD Thesis*, University of Leeds, 1977
- 12 Green, D. I., Orchard, G. A. J., Davies, G. R. and Ward, I. M. *J. Polym. Sci., B: Polym. Phys.* 1990, **28**, 2225
- 13 Ward, I. M. *Proc. Phys. Soc.* 1962, **80**, 1162
- 14 Troughton, M. J., Davies, G. R. and Ward, I. M. *Polymer* 1989, **30**, 58
- 15 Allen, S. R. and Roche, E. J. *Polymer* 1989, **30**, 996
- 16 Northolt, M. G. and van der Hout, R. *Polymer* 1985, **26**, 310
- 17 Takeuchi, Y., Yamamoto, F. and Shoto, Y. *Macromolecules* 1986, **19**, 2059
- 18 Li, T., Tashiro, K., Kobayashi, M. and Tadokoro, H. *Macromolecules* 1986, **19**, 1809
- 19 Alfrey, T. 'Mechanical Behaviour of High Polymers', Interscience Publishers, New York, 1948
- 20 Donald, A. M., Viney, G. and Windle, A. H. *Polymer* 1983, **24**, 155
- 21 Kwiatkowski, M. and Hinrichsen, G. *J. Mater. Sci.* 1990, **25**, 1548